High-speed wide-angle interleaved scanning technique for a 3D imaging lidar

NARASIMHA S. PRASAD,[1*] ANAND R. MYLAPORE [2]

[1]*National Aeronautics and Space Administration, Hampton, Virginia 23681*
[2]*AeroMancer Technologies Corporation, Washington, D.C. 20010*
**Corresponding author: narasimha.s.prasad@nasa.gov*

Received XX Month XXXX; revised XX Month, XXXX; accepted XX Month XXXX; posted XX Month XXXX (Doc. ID XXXXX); published XX Month XXXX

In this paper, we describe a novel interleaved scanner for an eye-safe 3D scanning lidar system to measure aerodynamic phenomena in a wind tunnel using elastic backscatter from seeding particles. The scanner assembly consists of a rotating polygon scanner for line scanning along the fast axis, a galvanometer (galvo) scanner for scanning along the slow axis, angular position sensors and motor controllers. The polygon scanner sweeps the lidar beam at up to 10,000 lines/s across a 27 deg angular field-of-regard in the fast axis, while the galvo scanner covers an angular range of 20 deg in the slow axis. Using this scanner, the lidar can perform non-intrusive flow visualization, velocimetry, and hard target mapping at mm-scale spatial resolution to a standoff range of 5 m at an update rate of 50 Hz for the full field-of-regard. An interleaved scanning methodology for the acquisition of two snapshots of 3D lidar intensity data with a 100 µs time offset is discussed. The design of the control and data acquisition electronics is described. The effects of rapid scanning on the response of a narrow field-of-view lidar are addressed. The design of the scanner is scalable and can be tailored to meet the requirements of other applications by increasing or decreasing the standoff range, angular field-of-regard and scan rate.

1. INTRODUCTION

Recent years have seen a rapid increase in the demand for and adoption of lidars for active 3D imaging in automotive, aerospace, and atmospheric sensing applications. Lidar measurements can be extended over a 3D field-of-regard using a flash lidar approach, a scanning approach, or a combination of the two. Flash lidars use a 2D focal plane array detector to simultaneously image the whole scene by measuring the backscatter from a laser beam that illuminates the field-of-regard. While the flash lidar approach can offer significant advantages in performance as well as size, weight, power and cooling (SWaP-C), the read-out speed of the current state of art in focal plane array detector technology restricts the maximum frame rate possible. This is a limitation for applications requiring the measurement of fast transient phenomena.

A variety of techniques are available to steer a narrow field-of-view (FOV) lidar beam along two orthogonal axes to cover a 3D field-of-regard. Mechanical scanners such as motorized rotation stages, gimbals, rotating polygons [1], galvanometers (galvos) [2] or Risley prisms [3] can steer beams over large optical angles with high optical efficiency that is only limited by the mirrors or transmissive optics used. Resonant scanners [4] offer faster steering speeds, but over narrow scan ranges and small aperture diameters. Recent advances in non-mechanical beam steerers such as optical phased array scanners [5], liquid crystal (LC) waveguides [6] or electrowetting approaches [7] offer the promise of increased scan speed, and reduced SWaP-C footprint. Other non-mechanical scanners such as acousto-optical or electro-optical crystal beam steerers can enable even faster scan speeds but are restricted to very narrow scan angles and small aperture sizes [8]. A common drawback of non-mechanical scanning technologies that use diffractive beam steering is lower optical efficiency compared to reflective or refractive approaches.

Here, we present a novel interleaved beam steering assembly that was developed for a prototype 3D picosecond scanning lidar for the investigation of 3D aerodynamic phenomena in wind tunnels. This lidar system uses a ~60 ps pulse-width, 1550 nm fiber laser operating at 10 MHz pulse-repetition-frequency (PRF) to illuminate a narrow divergence beam. The laser power emitted by the system is operationally ANSI Z136.1 Class IM eye-safe when the scanner is in use. A narrow FOV single-mode fiber-coupled optical receiver is used to collect the backscattered light along the line-of-sight and pre-amplified using an Erbium Doped Fiber Amplifier (EDFA) prior to conversion to an analog electrical signal by an 8 GHz bandwidth single-mode fiber detector. Narrow-band interference filters are used to filter out background light and EDFA noise. The lidar backscatter signal is digitized using an ultrafast analog-to-digital converter to obtain range-gated intensity data at mm-scale along the line-of-sight. By scanning this lidar beam along two orthogonal axes, the system obtains a time-accurate 3D intensity map of aerosols and hard surfaces in the field-of-regard at high spatial and temporal resolution. Spatially and temporally resolved

airspeeds are extracted using a 3D optical flow algorithm that cross-correlates the motion of aerosol features between successive frames.

More details on the design of this system and preliminary results obtained from laboratory and wind tunnel tests were presented in Refs [9,10]. A photograph of this system and preliminary results that were presented in [9,10] are summarized in Fig. 1.

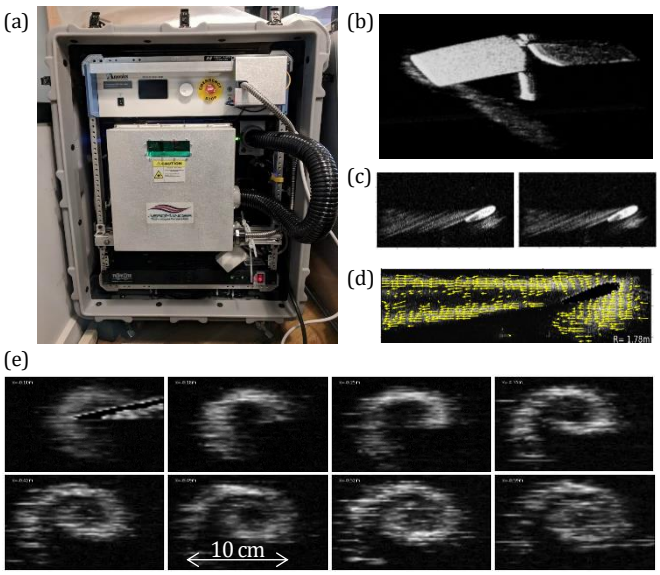

Fig. 1. (a) Front view of the 3D scanner lidar (from [9]), (b) Instantaneous 3D lidar backscatter image from a wing tunnel test of a wing stabilator test model with smoke seeding particles (from [9]), (c) Spanwise cross-sectional slices of the flow downstream of the wing from a pair of lidar sub-frames (from [9]), (d) 2D airspeed vectors extracted from the lidar sub-frame images (from [9]), (e) Lidar images showing the evolution of a wing tip vortex at different streamwise distances downstream of the wing (from [10]).

2. SCANNER DESIGN

This 3D airspeed sensing application requires the instrument to measure airspeeds as fast as 100 m/s with sub-cm resolution. Successive aerosol intensity images of the same 3D region with a time offset of ~100 μs or less are needed to capture the motion of aerosol features moving at an airspeed of 100 m/s to measure the airspeed profiles at the required spatial resolution. To accomplish this, we developed a novel interleaved scanning approach that enables the system to acquire two 3D images of the measurement volume with the required time offset in each frame. A two-axis scanner assembly with a high line-scan rate (~10,000 lines/sec), frame update rate (>50 Hz) and a wide scan angle (±13.5 deg in the fast axis and ±10 deg in the slow axis) is used for rapid scanning of the lidar beam along two axes, which is shown in Fig. 2. The scanner components are installed on an optical plate with a polygon scanner for fast line scanning; a galvo scanner for the slow axis; angular position sensors for each axis; a start-of-line (SOL) sensor for detecting the start of each polygon facet; a lidar transmit-receive (transceiver) assembly; and a turning mirror. The turning mirror is used to direct the lidar beam from the transceiver into the polygon mirror which scans the beam along the fast (horizontal) axis. A galvo scanner, which is used to scan the beam along the slow (vertical) axis, turns the beam to be orthogonal to the scanner mount plate. Both the polygon and galvo mirrors use protected gold coatings for ~97% reflection efficiency on each surface.

The specifications of the scanner are shown in Table 1. It should be noted that optical scan angles obtained from scanning a beam reflected off moving surfaces are twice that of the geometric angles. For the sake of consistency, all scan angles referred to henceforth will be the optical angles. The standoff range and scanning field-of-regard of the scanner were chosen to meet the requirements of this application, which is constrained by the wind tunnel test section dimensions in mid- to large-sized subsonic wind tunnels such as the 14- x 22-ft wind tunnel at NASA Langley Research Center and the 40- x 80-ft tunnel at NASA Ames Research Center.

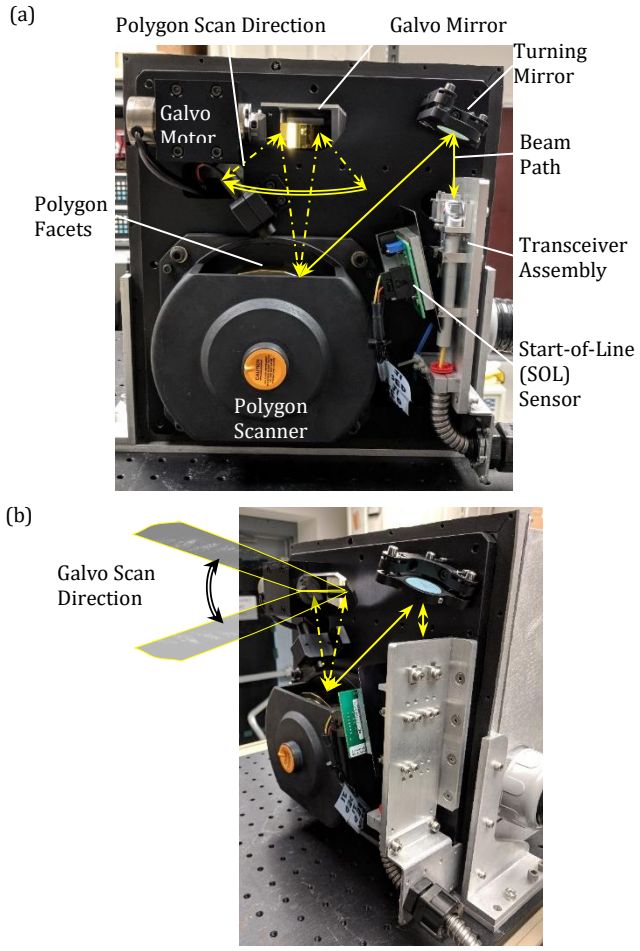

Fig. 2. Photographs of the two-axis lidar scanner with the parts labeled and the beam path shown in yellow: (a) Front view, (b) Angled view.

Table 1. Scanner Specifications.

Parameter	Value
Number of axes	2
Fast (horizontal) axis scanner	Polygon
Fast (horizontal) axis range	30 deg (~27 deg usable)
Fast (horizontal) axis speed	0-10,000 lines/s max.
Number of polygon facets	24
Polygon facet clear aperture	15 mm x 17 mm
Slow (vertical) axis scanner	Galvanometer

Slow (horizontal) axis range	20 deg max.
Fast (horizontal) axis speed	200 Hz (max)
Galvo mirror size	25 mm x 39 mm
Scan head size (H X D X W)	302 x 238 x 276 mm^3

3. SCANNING APPROACH

The polygonal scanner continuously scans the lidar beam along the horizontal axis at a maximum line scan rate of 10,000 lines/s. The polygon has 24 facets, where the vertical angle offset of individual facets have two different values alternating between 0 deg and -0.05 deg. Therefore, when the galvo scanner is turned off, the polygon scanner will scan along two parallel lines offset in vertical angle by 0.05 deg, as shown in Fig 3.

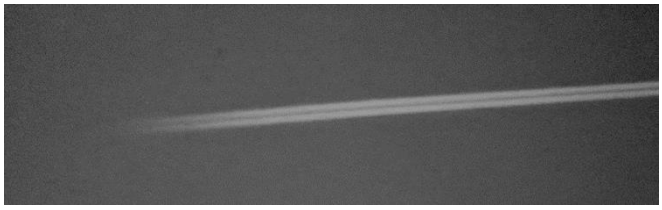

Fig. 3. Photograph of the polygon mirror beam scan pattern showing the lines scanned by adjacent facets, where the galvo scanner is not in operation.

When operated at its design condition, the galvo scanner scans at a constant speed of +500 deg/s in one direction and then retraces at the same speed in the opposite direction, i.e., -500 deg/s. This generates lines sloping slightly upwards in the positive direction and slightly downwards in the negative direction. At the design speed, each line will traverse a vertical angle of 0.05 deg in the galvo scan direction. Because of the 0.05 deg vertical angle offset between the adjacent facets, every alternate facet will retrace the path of the previous facet. The operation of the scanner is illustrated in Fig. 4(a) and 4(b) for the galvo scanning in the positive and negative directions, respectively. The scan pattern produced in this manner will result in two interleaved sub-frames that repeat the same number of lines that traverse the exact same spatial locations but are offset in time by 100 µs. The spacing between consecutive lines in each frame will be 0.1 deg. The number of lines in each frame can be adjusted by selecting the angular range of galvo motion. Setting the galvo scan range to 10 deg results in a maximum frame update rate of ~50 Hz. The frame rate and interrogation volume can be changed by adjusting the scan range.

In this scan pattern, there is minimal dead-time as the galvo continuously scans a triangular pattern. By multiplying or dividing the galvo scan speed by integer values, the spacing between the lines can be increased reduced proportionally, although it will come at the cost of temporal resolution, which might be acceptable for lower speed flow fields and slower phenomena. The scanner can also be operated at lower line scan rates for lower air speeds. While this will increase the spatial resolution of the aerosol images, it will result in a reduction in spatial resolution of measured airspeeds as shown in Fig. 4.

The reason for using a vertical offset on the polygon facets instead of using the galvo scanner to repeat each line is because the small angle step response time of the galvo scanner is on the order of 500 µs, which is much slower than the requirement.

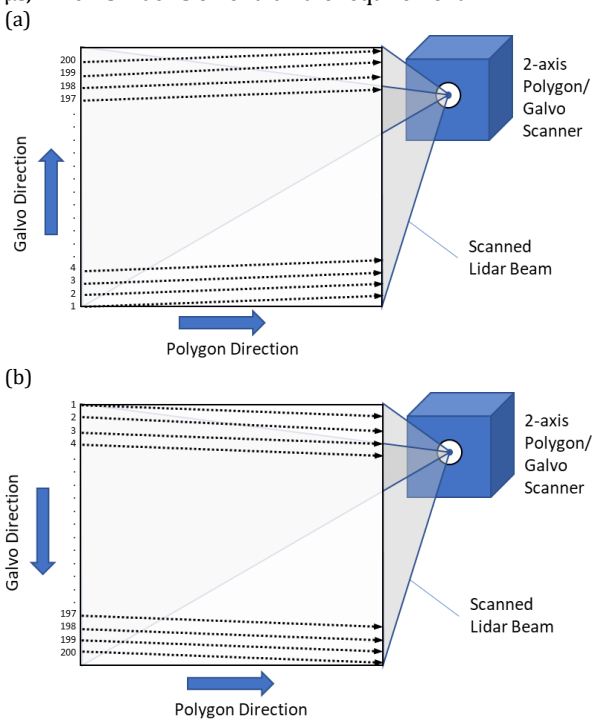

Fig. 4. Scan pattern produced by the galvo scanning in the (a) positive direction, (b) negative direction.

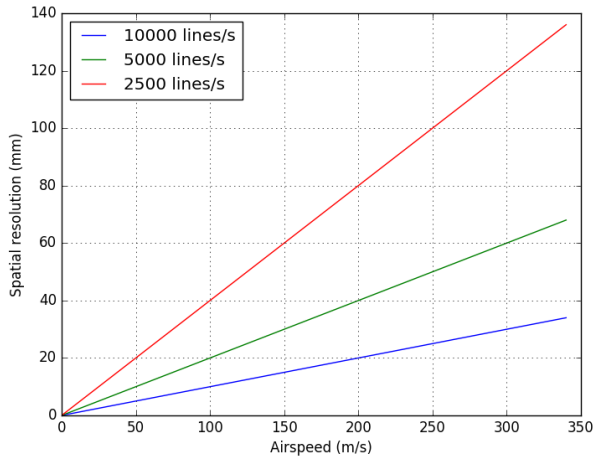

Fig. 5. Spatial resolution vs. airspeed for different line scan speeds.

Using a polygon scanner for beam steering along the fast axis has advantages over other mechanical scanning approaches such as resonant scanners, which can also provide high line-scan rates of >10,000 lines/second at low-cost. One advantage is that the polygon scanner provides linear response and constant scan speed along the line. The scan pattern for a resonant scanner has a sinusoidal profile, where the scan rate speeds up at the center of the scan area and slows down at the edges. As a result, the scan density for a resonant scanner is lower at the center of the scan area where more information is typically required. The scan direction for a polygon scanner is always in the same direction. Resonant scanners reverse the scan direction at the end of each line, thereby imparting opposite slopes to successive lines.

While this scanning method allows the lidar to measure relatively fast airspeeds at high resolution, care must be taken to align the fast axis with the direction of the free stream velocity to ensure that the aerosol features are captured in both instantaneous snapshots of backscatter intensity captured by the system in each frame. If the airspeed in the galvo scan direction is faster than the galvo speed, an aerosol feature that appears in the first image will disappear before the lidar scans the line again. However, this will not be an issue when the galvo scanner performs the slow scan in the opposite directions in the next frame.

4. SCANNER CONTROL

The system includes controllers for the polygon and galvo scanners and a data acquisition (DAQ) module to acquire scanner position data and to control the scanner parameters. The polygon and galvo motor controllers are used to power the motors, to provide motor control interfaces and to obtain motor position information.

The polygon motor controller enables the motor to be turned on or off using a digitally control input. The polygon motor can be operated either in internal mode at a speed of 10,000 lines/s, or it can be controlled externally using an external frequency input signal. The polygon motor position sensors include a quadrature encoder and a 1/rev signal. A digital sync out signal is enabled when the polygon motor stabilizes at the internally or externally programmed speed. The galvo scanner position sensor output is an analog voltage signal. The galvo motor's scan pattern is controlled using an analog voltage input. The SOL sensor consists of two components installed in the scanner: a laser source and a sensor module. The sensor sends out a digital signal at the beginning of each line of the polygon scanner and is connected to a digital input of the secondary DAQ system.

A multifunction USB data acquisition (DAQ) module is used to acquire position signals from the polygon and galvo scanners and to control the operation and speed of the scanner motors. This DAQ acquire an analog voltage signal from galvo position sensor via the galvo motor controller, a quadrature encoder input from the polygon motor encoder via the polygon motor controller, 1/rev signal from the polygon motor controller, a sync out signal from the polygon motor controller and a digital signal from the SOL sensor. The DAQ module also sends an analog output signal waveform to the galvo motor controller to control the galvo scanner, digital output pulses to the polygon motor controller to control the speed, a digital output signal to the polygon motor to turn it on or off, and a digital output signal to the polygon motor controller to select the internal or external operating mode.

In this system, the laser operates at 10 MHz PRF. During normal operation, the system acquires lidar waveform data at a trigger rate of 3.33 MHz. Because of bandwidth limitations, the scanner DAQ system acquires the position signals at 1.66 MHz as opposed to the 3.33 MHz waveform trigger rate of the digitizer module, i.e., every other lidar waveform. Because the position sensor signals are relatively slow and linear, as shown for the galvo position sensor data in Fig.6, the missing data can be interpolated to tag each lidar waveform array with polygon and galvo scanner position data.

An external clock module with subpicosecond jitter is used to synchronize the laser, DAQ, and scanner. The clock module supplies a 10 MHz trigger signal to the fiber laser, an external 10 MHz reference clock and a 3.33 MHz trigger signal to the lidar waveform digitizer, a 1.66 MHz trigger signal to the scanner DAQ module to synchronous the control and DAQ.

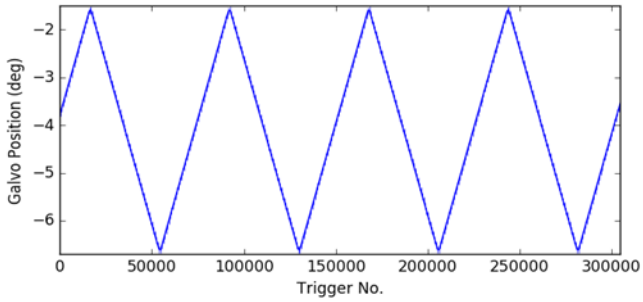

Fig. 6. Galvo position data shown as a function of sample number.

A software control package implemented in Python is used to control the operation of the scanner and for data acquisition, display and storage. The software allows the user to turn the scanner on or off, to specify the scan speed of the polygon and galvo motors and the angular range of the galvo scanner.

5. HIGH SPEED SCANNING EFFECTS

This lidar system uses a single-mode fiber laser collimator to emit a diffraction-limited beam with a divergence of ~1.5 mrad. The receiver also uses a single-mode fiber collimator with a very narrow acceptance angle of < 1 mrad. When this lidar beam is scanned rapidly, the overlap between the transmitter and receiver FOV reduces with an increase in distance away from the scanner. This is a result of a parallax error between the transmitter and receiver caused by relative motion between the transmit and receive axis during the time of transit of the laser beam to the target and back. The time (s) for light to travel from the laser to the measurement volume and back to the receiver can be expressed as 2 R/c, where R is the measurement range (m) and c is the speed of light (3×10^8 m/s). For a lidar beam swept by a polygon scanner at an angular scan rate of r_p (deg/s), the relative angular deviation, δ_θ, between the receiver and transmitter axis caused by polygon scanning is given by:

$$\delta_\theta = \frac{2R}{c}\frac{r_p \pi}{180} 2^M \qquad (1)$$

where, M is the number of mirrors or reflective optics between the receiver and the polygon mirror. The 2^M term in Eq. (1) is introduced to account for the fact that each reflective surface in the path will lead to a doubling of the angular deviation. In this system, there is one turning mirror in the receiver path. The polygon scanner sweeps a 30-deg optical angle in every line at a maximum scan rate of 10,000 lines/s. Therefore, the maximum value of r_p is 300,000 deg/s.

Figure 7 shows the variation in δ_θ as a function of range for different scan speeds, where the offset increases with distance from the instrument. This effect is more pronounced for the faster scan rates. Figure 8 illustrates the effect of this pointing offset by showing the ray tracing of the transmitted laser beam boundary and the receiver FOV when viewed orthogonal to the polygon scanner plane. For this analysis, the specifications of the laser and receiver collimator used in the 3D-LGAS system was applied. The receiver has a focusing lens of effective focal length of ~20 mm, which results in a effective receiver field diameter of 3.8 mm at the lens and FOV angle of 0.5 mrad. Figure 8(a) shows the case where the polygon

scanner is operated at the maximum speed of 300,000 lines/s, whereas Figure 8(b) shows the case where the polygon scanner is off, i.e., staring.

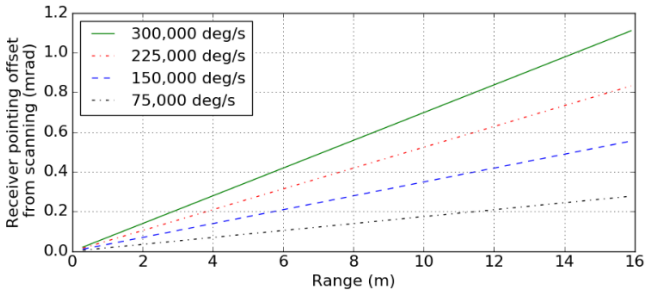

Fig. 7. Pointing offset, $\boldsymbol{\delta_\theta}$, in the receiver axis plotted as a function of range, R, for different polygon scan speeds.

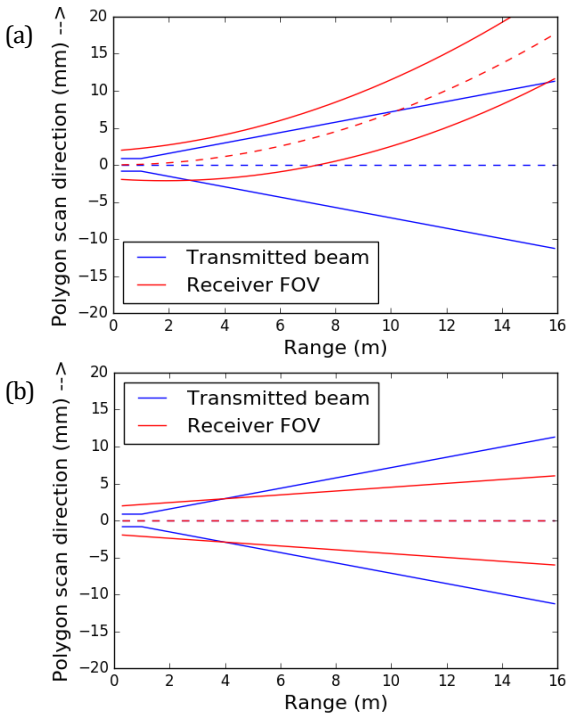

Fig 8. Comparison of scanning vs. stationary overlap between transmitted beam and receiver FOV as a function of range using geometric optics analysis assuming one turning mirror between receiver and polygon (a) 300,000 deg/s, (b) No scanning.

For evaluating this misalignment quantitatively, the relative signal loss caused by scanning, η_{scan}, is given by the ratio of the geometric lidar overlap between the scanning and staring cases.

$$\eta_{scan}(R) = \frac{OL_{scan}(R)}{OL_{stare}(R)} \qquad (2)$$

The scanning signal losses are plotted as a function of range for different polygon speeds in Figure 9. This analysis shows that when the polygon scanner is operated at maximum speed, the overlap between transmitter and receiver reduces to zero beyond 15 m.

The maximum range of unambiguous measurements ("wrap-around" distance) for a lidar can be expressed as:

$$R_{max} = {}^{c}/_{2f_L} \qquad (2)$$

where f_L is the laser PRF in hertz. For the 10 MHz PRF laser used in this system, R_{max} is 15 m.

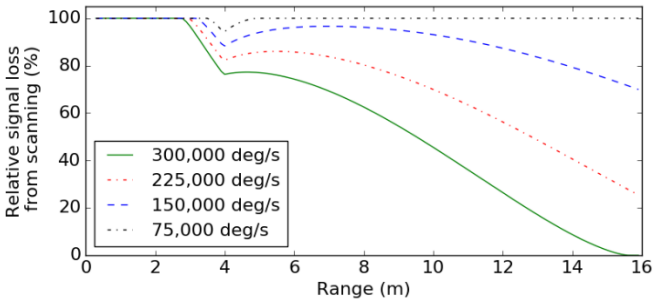

Fig 9. Relative signal loss calculated from geometric optics as a function of range caused by scanning using the polygonal scanner for a range of polygon speeds.

Therefore, any range ambiguity in the lidar return caused by hard targets or strong aerosol features beyond 15 m is eliminated by the high speed scanner. The maximum range of the instrument is constrained by the interplay of several variables including the laser PRF, the polygon scan speed, and the number of reflective surfaces in the path. It is possible to tailor the design of the instrument to meet the requirements of longer-range applications such as automotive lidars, which require a maximum detection range of several hundreds of meters. The detection range can be extended by using slower polygon scan speeds and lowering the laser PRF or by blocking the beam beyond the wrap-around range. Other ways to overcome this effect would be by eliminating the turning mirror in the receiver beam path or by introducing an offset angle in the relative alignment of the transmitter and receiver collimator to eliminate any overlap beyond the desired range at the scanning speed of interest.

6. CONCLUSIONS

We have developed an eye-safe 3D lidar scanning velocimeter for wind tunnel aerodynamic measurements and for the study of fast transient phenomena in large wind tunnels. The interleaved scanning approach described in this paper is a key enabling technology for our 3D scanning lidar, which allows it to investigate complex aerodynamic phenomena and to simultaneously characterize hard surfaces on the test model and wind tunnel boundaries at high resolution. The design of the scanner is scalable to larger or smaller fields-of-regard by modifying the polygon scanner geometry to increase or decrease the line scan rate or scan range. The angular range and scan speed of the galvo scanner can also be modified to meet the needs of the application. This scanning technology can be applied to meet the needs of emerging needs of aerospace and defense applications such as short- to mid-range aerial threat detection, urban air mobility and 3D range scanning. This interleaved scanning method can also be applied to other mechanical or non-mechanical beam steering techniques that combine fast and slow scanning axes or modes.

Funding. National Aeronautics and Space Administration (NNX15CL41P, NNX16CS81C, 80NSSC19C0645, 80NSSC19C0259).

Disclosures. National Aeronautics and Space Administration (E), ARM: AeroMancer Technologies Corporation (I, E)

Data availability. Data underlying the results presented in this paper are not publicly available at this time but may be obtained from the authors upon reasonable request.

References

[1] Beiser, Leo. "Design equations for a polygon laser scanner." *Beam Deflection and Scanning Technologies*. Vol. 1454. International Society for Optics and Photonics, 1991.

[2] Montagu, Jean. "Galvanometric and Resonant Scanners." *Handbook of Optical and Laser Scanning, Second Edition*. CRC Press, 2016. 418-473.

[3] Zhou, Yuan, et al. "Motion control of the wedge prisms in Risley-prism-based beam steering system for precise target tracking." *Applied optics* 52.12 (2013): 2849-2857.

[4] Holmström, Sven TS, Utku Baran, and Hakan Urey. "MEMS laser scanners: a review." *Journal of Microelectromechanical Systems* 23.2 (2014): 259-275.

[5] Hutchison, David N., et al. "High-resolution aliasing-free optical beam steering." *Optica* 3.8 (2016): 887-890.

[6] Davis, Scott R., et al. "Liquid crystal waveguides: new devices enabled by> 1000 waves of optical phase control." *Emerging Liquid Crystal Technologies V*. Vol. 7618. International Society for Optics and Photonics, 2010.

[7] Han, Wei, et al. "Transmissive beam steering through electrowetting microprism arrays." *Optics communications* 283.6 (2010): 1174-1181.

[8] Römer, G. R. B. E., and P. Bechtold. "Electro-optic and acousto-optic laser beam scanners." *Physics procedia* 56 (2014): 29-39.

[9] Mylapore, Anand R., Narasimha S. Prasad, and Sergiy Gerashchenko. "Development and Wind Tunnel Testing of a Novel 3D Scanning Lidar for Global Velocimetry." *AIAA Aviation 2019 Forum*. 2019.

[10] Prasad, Narasimha S., and Anand R. Mylapore. "Picosecond pulsewidth direct detection lidar for imaging applications." *Photonic Instrumentation Engineering VII*. Vol. 11287. International Society for Optics and Photonics, 2020.